**Steel and Composite Structures**, *Vol. 24, No. 3 (2017) 309-322*
DOI: https://doi.org/10.12989/scs.2017.24.3.309


# Composite action of notched circular CFT stub columns under axial compression

Fa-xing Ding [1], Bing Wen [1], Xue-mei Liu [2] and Hai-bo Wang [*1]

[1] *School of Civil Engineering, Central South University, Changsha, Hunan Province, 410075, P.R. China*
[2] *School of Civil Engineering and Built Environment, Queensland University of Technology, Brisbane, QLD 4001, Australia*

(*Received December 21, 2016, Revised March 08, 2017, Accepted March 30, 2017*)

**Abstract.** This paper conducted both numerical and theoretical studies to investigate the composite action of notched circular concrete-filled steel tubular (CFT) stub columns under axial compression and established a theoretical method to predict their ultimate bearing capacity. 3D finite element (FE) analysis was conducted to simulate the composite action and the results were in good agreement with experimental results on circular CFT stub columns with differently oriented notches in steel tubes. Parametric study was conducted to understand the effects of different parameters on the mechanical behavior of circular CFT stub columns and also the composite action between the steel tube and the core concrete. Based on the results, a theoretical formula was proposed to calculate the ultimate bearing capacity of notched CFT stub columns under compression with consideration of the composite action between the steel tube and the core concrete.

**Keywords:** circular concrete-filled steel tubular columns; notch; finite element analysis; ultimate bearing capacity; composite action

## 1. Introduction

In recent decades, extensive research has been done on circular concrete-filled steel tubular (CFT) stub columns by Chang *et al*. (2013a), Lu and Zhao (2010), Johansson and Gylltoft (2002), Huang *et al*. (2008), Park and Choi (2013), Xiamuxi and Akira (2011) and Wang and Chang (2013). The enhancement of structural properties for CFT columns is due to the composite action between individual constituent elements. The steel tube acts as reinforcement and provides a confining pressure to concrete, meanwhile the steel tube is stiffened by the concrete. However, imperfections always exist in the outside steel tube of CFT members, which may impair the composite action between the steel tube and concrete and reduce the structural integrity and service life of the composite members. The imperfections in the steel tube generally include: geometric imperfection and material imperfection. The material imperfection is mainly related to defects or thickness variations by the corrosion, welding or other chemical corrosion (Chang *et al*. 2013b).

The material imperfections of constructional steel and cylindrical steel structures have been intensively researched in recent years. Melchers (2006) analyzed different factors that influence the corrosion rate of structural steel immersed in seawaters. Bhandari *et al*. (2015) presented corrosion and notch problems of the structural steel, and the influence of corrosion and notches on the behavior of steel were analyzed. Sultana *et al*. (2015) investigated the behavior and ultimate compressive strength of steel plates and stiffened panels with different depth of pitting corrosion with element modelling method. Jullien and Limam (1998) studied the bearing capacity and bulking model of cylindrical shells under axial compression with various shapes, sizes and locations of notches in the steel. Javidruzi *et al*. (2004) investigated the vibration, bulking and dynamic stability of the notched cylindrical shells under tension and compression. Han *et al*. (2006) investigated the influence of punched openings in the aluminum cylinders based on the experimental and numerical methods.

As an attempt to further investigate the influence of the local material imperfections of steel tube on the mechanical performance of circular CFT columns under axial compression, the artificial notches through-out the wall thickness of steel tube were always used to represent the material imperfections from corrosion or other damages. Yu *et al*. (2007) investigated the mechanical behavior of the circular CFT columns with and without notches in the steel tube. The results on the load-strain ratio curves of the steel tubes suggested that once a steel tube was notched with small holes in the mid-height region, the confinement effect was enhanced while the axial compressive stiffness was reduced. However, the ultimate capacity and residual capacity were hardly influenced. Chang *et al*. (2013b) conducted 15 notched circular CFT stub columns under axial compression to investigate the influence of notch length, notch orientation, concrete strength and steel ratio on the mechanical properties of the columns. The results indicated that the notched CFT specimens had lower mechanical performance than those intact CFT specimens due to that notch steel tube could not offer sufficient confinement on the concrete core. Besides, an empirical

*Corresponding author, Ph.D.,
E-mail: haibarg@163.com

**Copyright © 2017 Techno-Press, Ltd.**

ISSN: 1229-9367 (Print), 1598-6233 (Online)

equation for predicting the strength of a notched CFT column was proposed based on regression analysis.

However, available studies on notched CFT columns are very limited and further investigation is needed for some important issues, one of which is the composite action between the steel tube and the core concrete, as well as the composite action degradation due to the notches in steel tubes with different orientation and quantities. Besides, currently there is no unified formula for predicting the bearing capacity of notched CFT columns under axial compression.

This paper, therefore, aims to thoroughly study the composite action between the steel tube and the core concrete of circular CFT stub columns with different notches in steel tubes under axial compression. A theoretic formula was also proposed to predict the bearing capacity of such columns. This paper starts with the establishment of 3D FE models of circular CFT stub columns with notch in steel tubes under axial compression using ABAQUS software package. The models were validated by existing experimental results. The next section presents finite element analysis (FEA) on the mechanical behavior and composite action of circular CFT stub columns with axial notch, circumferential notch and inclined notch in steel tubes respectively. The subsequent section conducts parametric study to understand the impacts of different parameters on the mechanical behavior of the columns. And at last, a practical and unified computation formula with consideration of the composite action to predict the ultimate bearing capacity of CFT stub columns with notch in steel tubes is proposed and presented.

## 2. Finite element modeling

### *2.1 Finite element models*

In this study, FE models were established by using the nonlinear finite element package ABAQUS/Standard 6.4 (2003). Eight-node reduced integral format 3D solid elements were used to model the steel tube, core concrete and loading plate. A structured meshing option was adopted of which the element shape is hexahedron, and the resulting FE model is shown in Fig. 1. In the FE models, a surface to surface contact was adopted for the interaction of steel tube and core concrete, of which the inner surface of steel tube was the master surface as well as the external surface of core concrete as the slave surface. Limited glide was adopted for Glide formula while the discretization method was surface to surface, and the "adjust only to remove overclosure" option was used in order to prevent any overclosure that could occur. Normal behavior and tangential behavior were used in contact property to simulate the bond-glide action between steel tube and core concrete. The normal behavior was set as "hard" contact, which allows separation after contact. The "penalty" function formulation was chosen for the tangential behavior. The friction coefficient between the steel tube and the core concrete was indicated to be from 0.3 to 0.6 in existing research conducted by Baltay and Gjelsvik (1990). In this study, a friction coefficient of 0.5 was adopted thereby, which was proved to be rational in the prior research by (Ding *et al*. 2011a).

A tie constraint may couple two separate surfaces together so that no relative motion occurs between the surfaces. Therefore, the tie option was adopted for the constraint between steel tube, core concrete and loading plate. The loading plate was the master surface as well as the end face of steel tube and core concrete was the slave surface. Such arrangement will allow the load transfer from the loading plate to the steel tube and core concrete, and also enable them to bear load at the same time. Rigid surface was used to simulate the loading plate where the modulus of elasticity was taken as $1.0\times10^{11}$ and the Poisson ratio was set to be $1.0\times10^{-7}$.

A triaxial concrete model of the core concrete in CFT columns with the circular or polygonal cross-section under axial compression proposed by Ding *et al*. (2011a), which is a modified model presented by Ottosen and Ristinmaa (2005), was adopted in the model

$$y=\begin{cases}\dfrac{kx+(\mathrm{m}-1)x^2}{1+(k-2)x+mx^2} & x\le 1\\ \dfrac{x}{\alpha_1(x-1)^2+x} & x>1\end{cases} \tag{1}$$

where $k$ is the ratio of the initial tangent modulus to the secant modulus at peak stress and equals to $9.1f_{cu}^{-4/9}$, $m$ is a parameter that controls the decrease in the elastic modulus

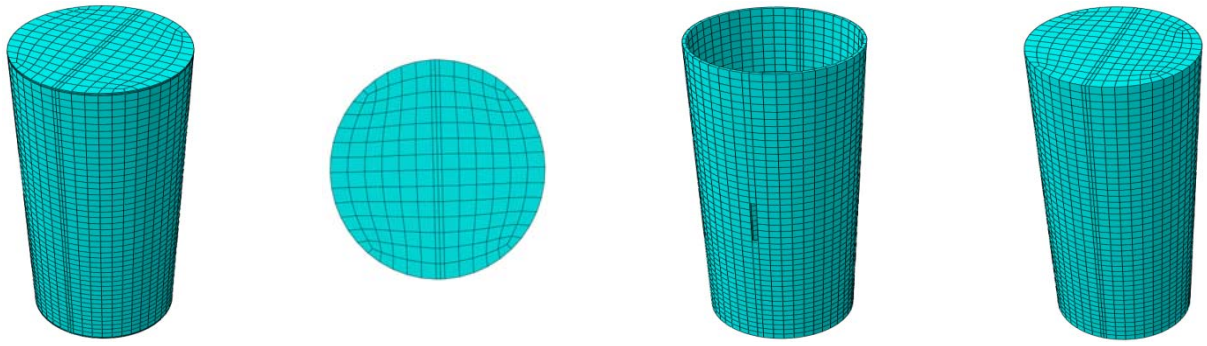

(a) Finite element model (b) Loading plate model (c) Steel tube model (d) Concrete model

Fig. 1 Mesh generation of model

along the ascending branch of the axial stress-strain relationship and equals to $1.6(k\text{-}1)^2$. For a CFT stub column, parameter $\alpha_1$ can be taken as 0.15. More information of the concrete model could be referred by Ding *et al*. (2011a).

The triaxial concrete model adopted in this paper is based on the stress-strain relation of concrete under uniaxial stress, together with the parameters of strength criterion of concrete under multi-axial stresses and other parameters stated in the paper. This model is suitable to simulate the stress-strain relation of concrete under uniaxial, biaxial and triaxial stress. The concrete model was also validated for modelling circular, square and octagonal sectional CFT columns (Ding *et al*. 2017, 2016a and b). The parameters in ABAQUS were defined by Ding *et al*. (2011b): the eccentricity is 0.1; the ratio of initial equibiaxial compressive yield stress to initial uniaxial compressive yield stress ($f_{b0}/f_{c0}$) is 1.225; the ratio of the second stress invariant on the tensile meridian to that on the compressive meridian is 2/3; the viscosity parameter is taken as 0.005; and the dilation angle is 40°.

With above parameters available and the above concrete model, in which the composite action between the core concrete and the steel tube is considered, is suitable for numerical analysis on tri-axial-compressed concrete in CFT columns with notches in steel tube.

An elasto-plastic model, considering Von Mises yield criteria, Prandtl-Reuss flow rule, and isotropic strain hardening, was used to describe the constitutive behavior of steel. The expression for the stress-strain relationship of steel is as follows by Ding *et al*. (2011a)

$$\sigma_{\mathrm{i}}=\begin{cases}E_{\mathrm{s}}\varepsilon_{\mathrm{i}} & \varepsilon_{\mathrm{i}}\le\varepsilon_{\mathrm{y}}\\ f_{\mathrm{s}} & \varepsilon_{\mathrm{y}}<\varepsilon_{\mathrm{i}}\le\varepsilon_{\mathrm{st}}\\ f_{\mathrm{s}}+\zeta E_{\mathrm{s}}(\varepsilon_{\mathrm{i}}-\varepsilon_{\mathrm{st}}) & \varepsilon_{\mathrm{st}}<\varepsilon_{\mathrm{i}}\le\varepsilon_{\mathrm{u}}\\ f_{\mathrm{u}} & \varepsilon_{\mathrm{i}}>\varepsilon_{\mathrm{u}}\end{cases} \tag{2}$$

where $\sigma_i$ is the equivalent stress and $f_u$ equals to $1.5f_s$, which corresponds to the yield strength. $E_s$ is taken to be $2.06\times10^5$ MPa. $\varepsilon_i$ is the equivalent strain, while $\varepsilon_y$ is the strain when steel yields. $\varepsilon_{st}$ is the strain when steel reinforcement equals to$12\varepsilon_y$. $\varepsilon_u$ is the strain when the steel reaches ultimate strength and equals to $120\varepsilon_y$, and $\zeta$ equals to 1/216. The Prandtl-Reuss flow rule, which can be applicable to three-dimensional stress analysis, is used to the constitutive relationship of the steel tube, for the elastic part is considered into the increment in strain during the process of plastic deformation.

Load was applied through increments of displacement and both material and structural nonlinearities were considered and solved using the incremental iterative method.

### 2.2 Model validation

The FE models are used to simulate the behavior of circular CFT stub columns with different notches in steel tubes under axial compression and validated through the experimental work conducted by Yu *et al*. (2007) and Chang *et al*. (2013b). The different notch orientation is shown in Fig. 2, where $l_0$ is the longer side of notch, $b$ is the shorter side of notch, $\theta$ is the angle between inclined notch and axial direction of specimen, and $\beta = l_0/D$ ($D$ is the diameter of steel tube) is length to diameter ratio of notch.

The compression behavior of the CFT columns obtained from the FE models was validated with the compression test performed by Yu *et al*. (2007) and Chang *et al*. (2013b). The average ratios of the test results over the FE modelling results are shown in Table 1, where the results obtained from the FE modelling are in good agreement with the test results.

The typical comparisons of load-strain curves between FE results and experimental results for axial, circumferential and inclined notched specimens under axial compression are shown in Figs. 3, 4 and 5, respectively. It can be found from Fig. 3 to Fig. 5 that the ultimate bearing capacity of modelling results and test results achieved good agreement, while the stiffness of the stub column obtained from test results was slightly smaller than that of the FE modelling results. The deviation of the stiffness between the two curves might be caused by the different displacement measurement methods adopted in test and FE modelling. The deformation of the test specimens was measured by two gauges attached at the end of the specimens which included the end constraining effects at the top and bottom

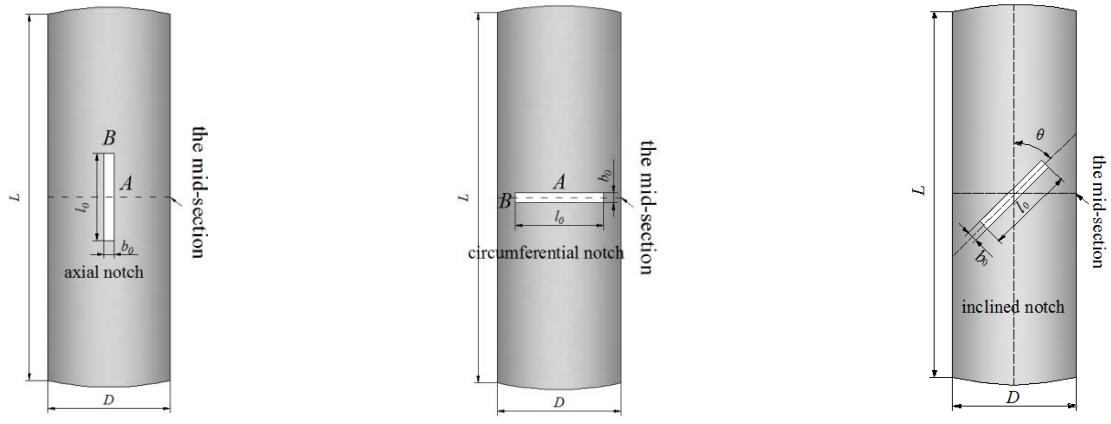


(a) Axial notch (b) Circumferential notch (c) Inclined notch

Fig. 2 Configuration of different notches in steel tubes of CFT column

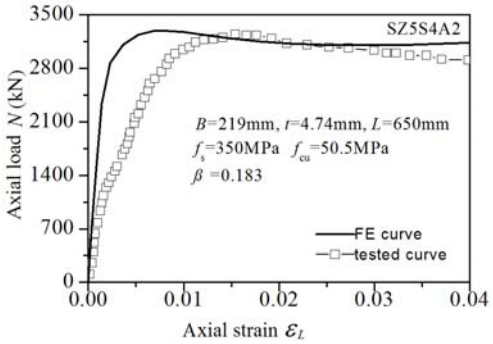


(a) Tested results of specimen SZ5S4A2

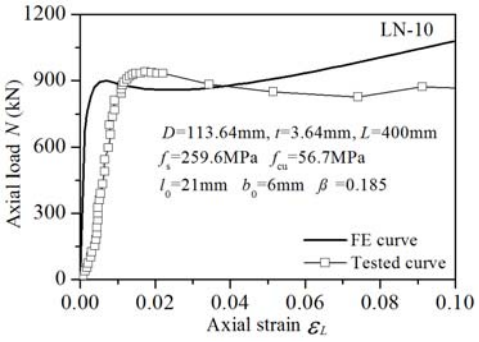


(b) Tested results of specimen LN-10

Fig. 3 Comparisons between FE and tested curves of axial notched specimens

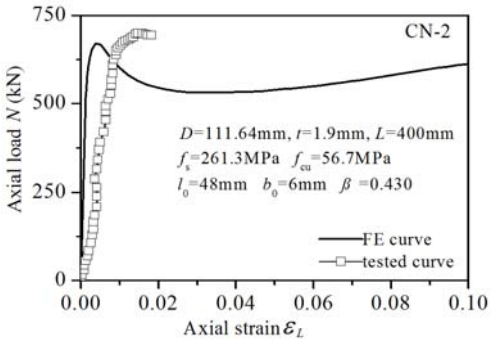


(a) Tested results of specimen CN-2

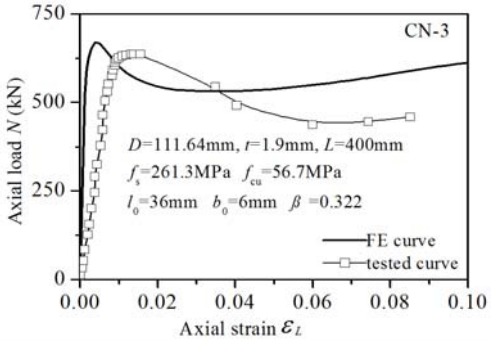


(b) Tested results of specimen CN-3

Fig. 4 Comparisons between FE and tested curves of circumferential notched specimens

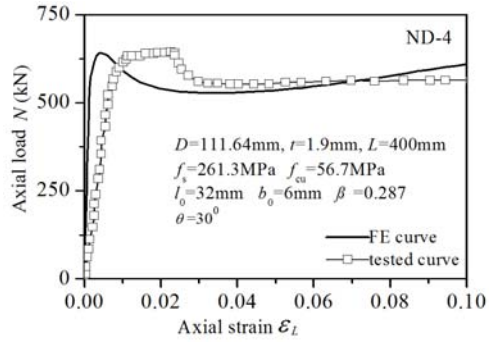


(a) Tested results of specimen ND-4

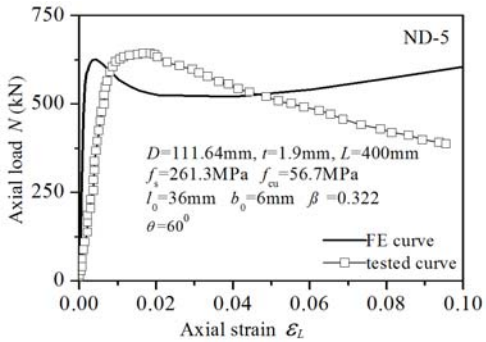


(b) Tested results of specimen ND-5

Fig. 5 Comparisons between FE and tested curves of inclined notched specimens

of the specimens. This may result in the higher measured deformation of test specimens than those of the FE modelling results. The difference was justified in Yu *et al.* (2007) by conducting the contrast experiment of four different deformation measurement methods.

## 3. Composite action analysis

### *3.1 Effect of length to diameter ratio of axial notch*

Full scale FE models of circular CFT stub columns with different axial notch length to diameter ratios were established to investigate the composite action between the steel tube and the core concrete. The nominal dimension of each specimen was 500($D$) mm × 10($t$) mm × 1500($L$) mm, where $D$ is the external diameter. $t$ is the wall thickness of the steel tube and $L$ is the height of specimen. Concrete strength $f_{cu}$ was 60 MPa and steel strength $f_s$ was 345 MPa. A rectangular notch was slotted at the mid-height region of steel tubes with the length $l_0$ in the axial direction with a size of 75 mm, 150 mm, 225 mm, 300 mm, 375 mm, or 450 mm respectively (with $\beta$ values at 0.15, 0.3, 0.45, 0.6, 0.75, and 0.9, respectively) and the width $b_0$ of the notch with a size of 20 mm ($b_0$ = 20 mm can be seen as the bigger width of the notch. When $b_0$ < 20 mm, the mechanical behavior of circular CFT stub columns is hardly influenced based on full scale FE models). And, in addition, FE model of an

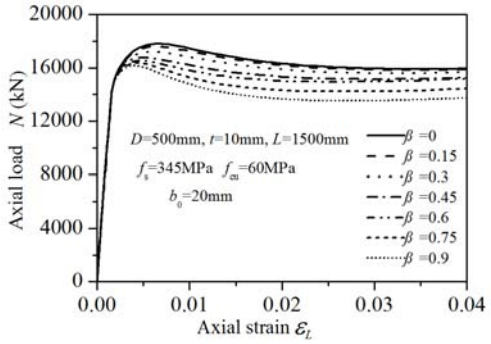


Fig. 6 Effect of different notch length to diameter ratio on the load-strain curve of axial notched specimens

intact tube was established and simulated for comparison.

The effect of different length to diameter ratio on the load-strain curve of axial notched specimens is shown in Fig. 6. It can be seen that the stiffness of the composite CFT column were generally the same when specimens were in the elastic phase. With the increase of the length to diameter ratio, the ultimate bearing capacity and residual bearing capacity of the specimens decreased continuously.

Seen from the stress contours at mid-section for concrete of axial notched specimens with different length to diameter ratio at the ultimate state in Fig. 7, the stress of concrete declines from the central section to the surrounding area under ultimate state and the center of the

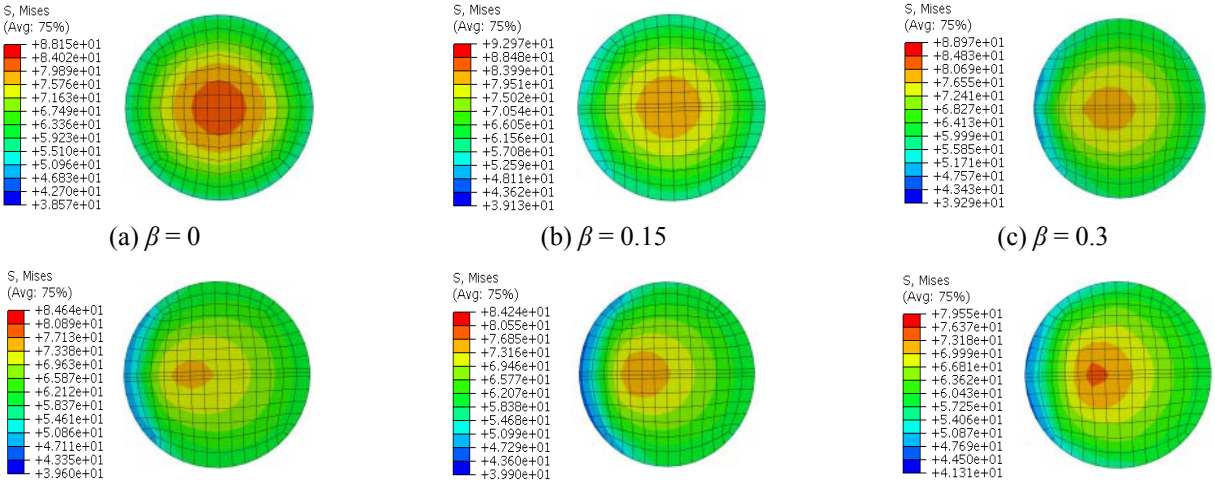


(a) $\beta = 0$ (b) $\beta = 0.15$ (c) $\beta = 0.3$

(d) $\beta = 0.45$ (e) $\beta = 0.6$ (f) $\beta = 0.9$

Fig. 7 Stress contours of mid-section in concrete of axial notched examples with different notch length to diameter ratio at ultimate state

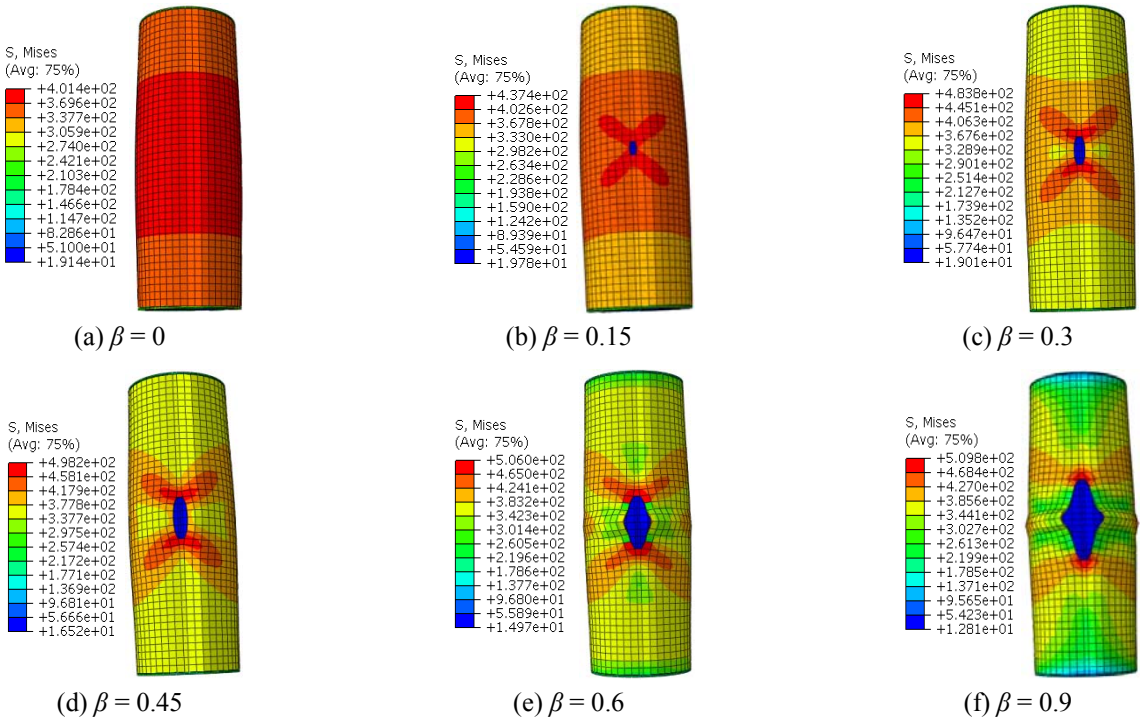


(a) $\beta = 0$ (b) $\beta = 0.15$ (c) $\beta = 0.3$

(d) $\beta = 0.45$ (e) $\beta = 0.6$ (f) $\beta = 0.9$

Fig. 8 Breakdown stress contours of examples with different notch length to diameter ratio

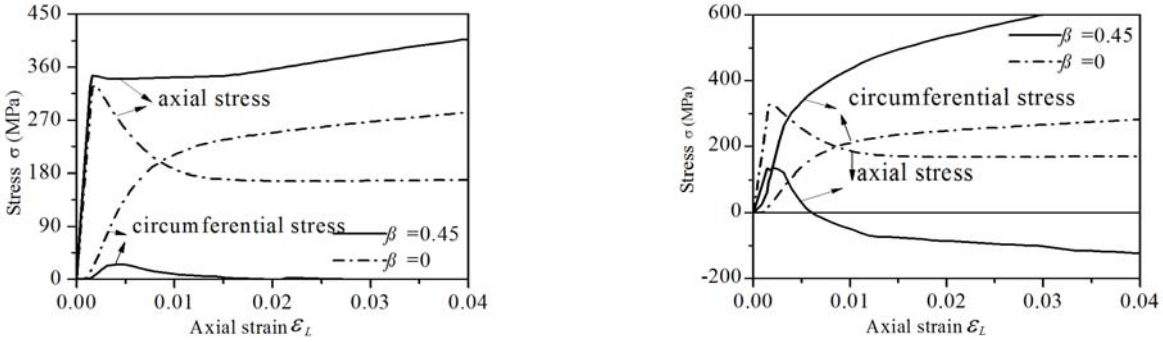


(a) Middle of the notch long side (b) Middle of the notch short side

Fig. 9 Steel stress-strain in the middle of axial notched sides

maximum stress of the concrete was found to be moved to the notch area. Furthermore, the longer the notch length was, the larger the movement would be. And the global stress of mid-section of the concrete decreases with the increase of notch length.

The breakdown stress contours of selected examples with different notch length to diameter ratio is shown in Fig. 8, It was observed that the buckling of steel tube at the mid-section of specimens became more severe with the increase of notch length. When the notch length reached 300 mm, the buckling deformation of steel tube was observed to be large when the specimen broke down and the steel tube had been found to be separated from the concrete. With the increase of notch length, the stress of the steel tube at notched region was more uneven, with stress concentration appearing at the shorter side of notch and its corner. The longer the notch was, the more severe the stress concentration was.

According to Ding *et al*. (2011b), the stress-strain curve can reflect the strength of composite action. If the axial stress-strain curve intersects with the circumferential one in the process of loading, the steel tube will provide confinement effect on the core concrete. Therefore, the axial and circumferential stresses of unit integral point A and B in the steel tube and the average axial stress in the mid-section of the concrete were extracted. The locations of A and B can be found in Fig. 1.

Fig. 9 shows the typical stress-axial strain curve for steel at the mid-section of the longer side and the shorter side of the notch with the notch length at 225 mm in comparison to that at the same place without notch. It should be mentioned that the axial compressive stress and the circumferential tensile stress were considered a positive sign in the figure.

It can be seen from Fig. 9(a) that at the early stage of loading, the mid-section of the longer side of the notch only bore axial compressive stress and then changed to bear both axial compressive and circumferential tensile stresses. However, the circumferential stress declined gradually and the notched steel tube at the mid-section bore axial compressive stress only at the later stage of loading. Therefore, the axial and circumferential stress-strain curves have no intersection compared with the intact CFT column and the steel tube along the longer side of the notch mainly acted to resist axial compression instead of providing constraints for the core concrete.

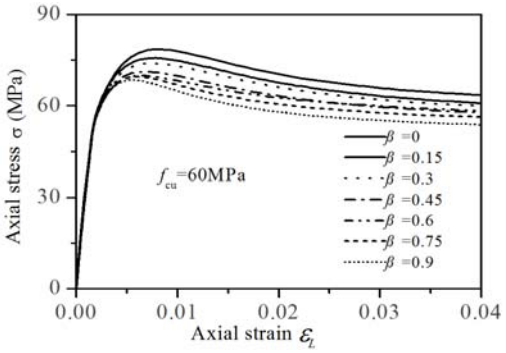


Fig. 10 Impact of different notch length to diameter ratio on average axial stress-strain curve of concrete in the middle section of specimens

At the same time, in Fig. 9(b), the axial stress in the mid-section of the shorter side of the notch started with the state of compression and then changed to the state of tension. While the circumferential tensile stress in the mid-section for the shorter side of notch grew rapidly and intersected with the axial stress curve. In the later period, the circumferential tensile stress increased much greater than its yield strength and the steel tube was subjected to biaxial tensile stress. Therefore, the steel tube at the shorter side of notch had the main effects on constraining the concrete but contributed little to resist axial compression at the later period of loading.

Such mechanism results from the stress-strain curve for steel at the mid-section of the longer side and the shorter side of the notch indicates that due to the discontinuity of the steel along the axial and circumferential direction of the notch, the stress transferring path of the notched steel tube were greatly changed. The steel of longer side of the notch only resists axial compression while the steel of short side of the notch mainly constrains the core concrete.

The effect of different length to diameter ratio of notch on average axial stress-strain curve of concrete in the mid-section of specimens is shown in Fig. 10. It can be seen that the maximum values of average axial stress of concrete is much larger than concrete's axial compressive strength (60 MPa) which stated that steel tube still had constraint effects on core concrete. However, with the increase of the notch length, the average axial stress of concrete decreased

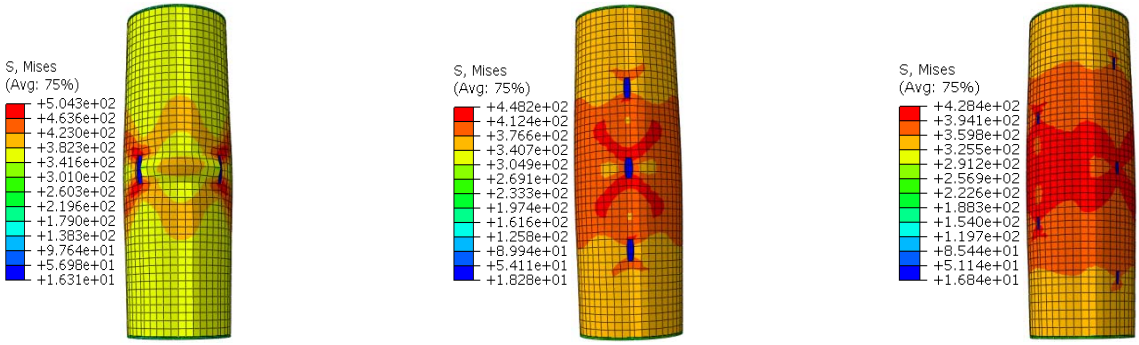


(a) $n = 2$ (b) $n = 3$ (c) $n = 5$

Fig. 11 Failure stress contours of different axial notch quantity and location of specimens

continuously, which showed that the composite action for concrete decreased continuously with the increase of notch length.

### *3.2 Effect of axial notch quantity and notch location*

Full scale FE models were established with the consideration of different axial notch quantity and notch location in this section to investigate the composite action between the steel tube and the core concrete. The nominal dimension of each specimen was 500($D$) mm × 10($t$) mm × 1500($L$) mm. Concrete strength $f_{cu}$ was 60 MPa and steel strength $f_s$ was 345 MPa. The holistic notch length to diameter ratio $\beta$ of specimen was the superposition of each notch length to diameter ratio and was chosen to be 0.6. The holistic length of notch was 300 mm. Notch quantity $n$ considered for this study was 1, 2, 3, and 5, respectively, corresponding to the length of a single notch being 300 mm, 150 mm, 300 mm, and 60 mm respectively. The notch location was changed for each specimen and the results were compared with that of the model without notch. Breakdown stress contours of the CFT column with 2, 3, and 5 notches are shown in Fig. 11. Breakdown stress contours of those with a single notch and without notch can be seen in Fig. 8. It was observed that stress distribution was becoming more even with the increase of the notch quantities when the specimen was broken down and the stress concentration was weakened.

Fig. 12 shows the load-axial strain curve of the specimens with different axial notch quantity ($n$) and notch location. It can be seen, different notch quantity and notch location have no effect on stiffness of the specimens but only affected the bearing capacity of the specimen slightly when $\beta$ was the same at 0.6. The bearing capacity of the specimens with single notch in the mid-section of steel tube is the lowest. However, the bearing capacity of specimens with other notch quantities at 2, 3, or 5 and different location were similar and their bearing capacity was also falling in between that of the specimen with a single notch in the mid-section of steel tube and the specimen without any notch. It could be concluded that multiple axial notches could be considered with equivalence to a single axial notch with a notch length equal to the superposition of the notch length of all axial notches as well as the composite action between the steel tube and the concrete.

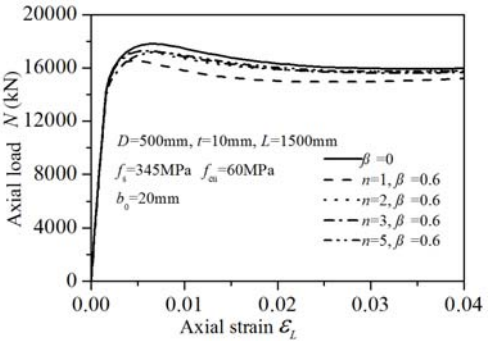


Fig. 12 Effect of notch quantity and location on load-strain response of axial notched specimens

### *3.3 Effect of length to diameter ratio of circumferential notch*

Full scale FE models with different circumferential notch length to diameter ratios were established to investigate the composite action between the steel tube and the core concrete. In the FE models, the nominal dimension used for the models were the same as those established in Section 2.2 with the same concrete and steel strength. A circumferential notch was slotted at the mid-height region of steel tubes. The notch length was the arc length of the notch. Different notch length were investigated at 0, 0.1$D$, $\pi D/4$, $\pi D/2$, $3\pi D/4$, or $\pi D$ corresponding to different $\beta$ value at 0, 0.1, $\pi/4$, $\pi/2$, $3\pi/4$, or $\pi$ respectively. The $\beta$ value 0 and $\pi$ corresponded to the specimens without notch and with a circumferential notch.

From the load-axial strain curve in Fig. 13, it can be seen that the stiffness of the composite CFT column decreased slightly in the elastic stage while the ultimate bearing capacity of the specimen increased as well as residual bearing capacity with the increase of notch length. It indicates that the circumferential notch reduced the stiffness of the circular CFT stub columns but increased the bearing capacity slightly. With the increase of the circumferential notch length, more steel tubes in the mid-section of the specimen contribute to confine the core concrete instead of bearing the axial compression due to the discontinuity of the steel. Such mechanical properties of the circumferential notched specimens tend to be similar with those of steel tube confined concrete (STCC) stub columns,

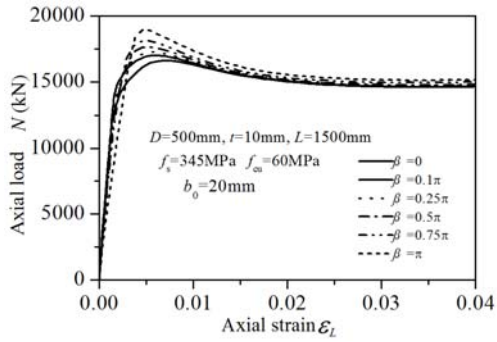


Fig. 13 Effect of notch length on load-strain response of circumferential notched specimens

which own slightly higher ultimate bearing capacity and smaller stiffness than the CFT counterparts. This property was also confirmed by the experiment conducted by Han *et al*. (2005) and Yu *et al*. (2007).

Fig. 14 shows the stress contours at the mid-section of concrete for the specimen with different circumferential notch length at ultimate state, the contours shows that when the bearing capacity was in limit state, the maximum stress in the mid-section of concrete would be transferred from the mid-section of concrete without notch to the section of that with notch, the stress of the concrete around the notch being greater than the other part which indicated the stress concentration phenomenon, and the overall stress of

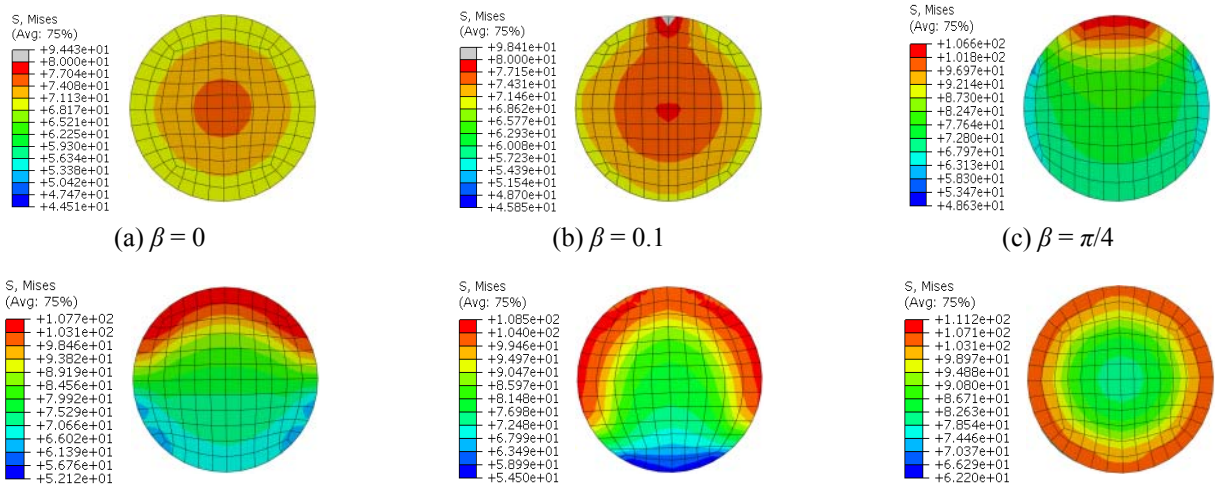


Fig. 14 Stress contours on the middle section of concrete when the specimen with different circumferential notch length at ultimate state

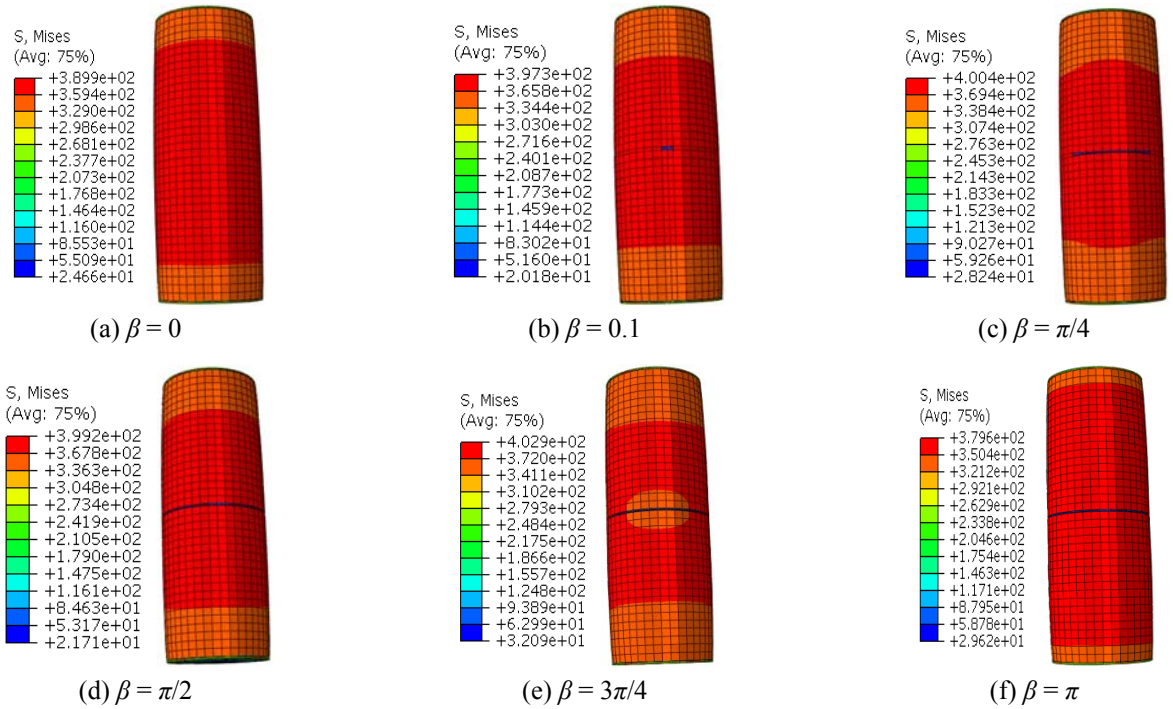


Fig. 15 Breakdown stress contours of specimens with different circumferential notch length

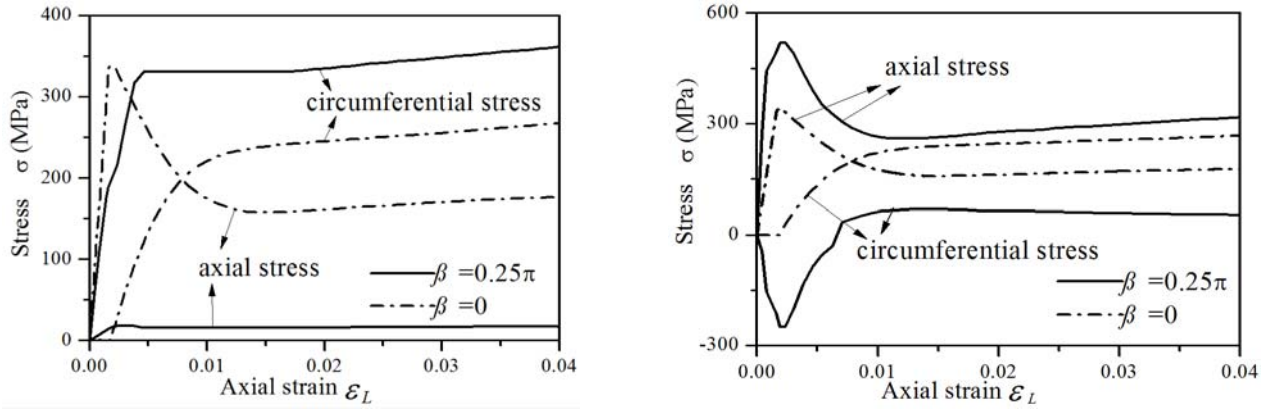


(a) Middle of the longer side of notch (b) Middle of the shorter side of notch

Fig. 16 Stress-strain curve on steel tube unit at the middle of the longer side and the shorter side of notch

concrete increased slightly with the increase of notch length.

Fig. 15 shows breakdown stress contours of specimens with different circumferential notch length. It also indicates that the stress distributions of the breakdown specimens with different circumferential notch length were similar with that of the specimen without notch, stress concentration phenomenon was not observed.

The stress- axial strain curves at the mid-section of the longer and shorter side of notch of the specimens where the circumferential notch length was $\pi D/4$ are shown in Fig. 16. As can be seen, in the earlier period, circumferential stress in the mid-section of the longer side of notch grew quickly while axial stress was very small which means that the steel tube at longer side of notch mainly provide the constraint effects on concrete. What is more, when loading begins, the steel tube at shorter side was in a state of bi-directional compression and finally the axial stress decreased gradually and tended to become stable, while the circumferential compressive stress decreased to zero gradually, and hence the steel tube was in a uniaxial compression state which indicates that the steel tube at the shorter side merely bear axial compression during the later period.

Fig. 17 shows the average axial stress-strain curve for the mid-section of concrete with different circumferential notch length. As the figure shown, average axial stress of mid-section of the concrete became larger with the increase of circumferential notch length which can be explained by the enhanced composite action of the steel tube confined concrete (STCC) stub columns.

With the analysis results above of the composite action between the steel tube and the core concrete with axial and circumferential notches at the mid-section of the steel tube, it can be concluded that the composite action is reduced with axially slotted notch but enhanced with circumferentially slotted notch.

### *3.4 Effect of inclined notch angle*

Full scale FE modelling of circular CFT stub columns with different inclined angle ($\theta$) notches were conducted and also compared with specimens with axial and circumferential notches to investigate the composite action between the steel tube and the core concrete. The same concrete and steel strengths as the above sections were used for modelling. The nominal dimension used for the models were also the same as those used in the above sections at 500($D$) mm × 10($t$) mm × 1500($L$) mm. A inclined notch was slotted at the mid-height region of steel tube. $\theta$ is the angel between the notch orientation and the axial orientation of the specimens as shown in Fig. 1(c). Different notch angel $\theta$ at 0°, 30°, 45°, 60°, and 90° (0° and 90° were representing specimens with axial and circumferential notch respectively) were included for the investigation. And the typical notch length was taken as 0.5$D$ (250 mm) and the

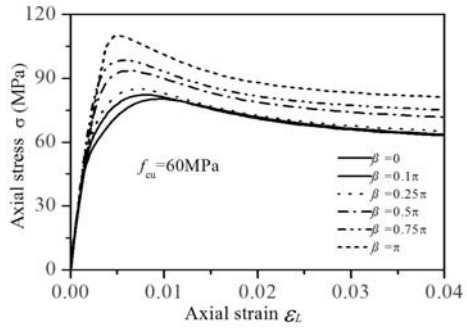


Fig. 17 Average axial stress-strain curve of the concrete of middle section in specimens with different circumferential notch length

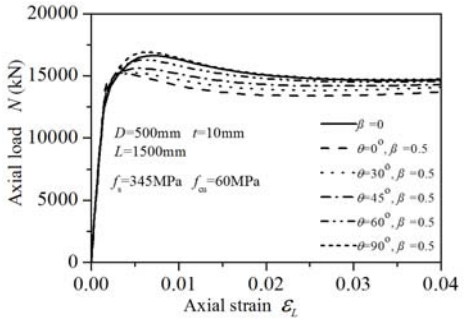


Fig. 18 Load-axial strain curve of specimens with different notch orientation

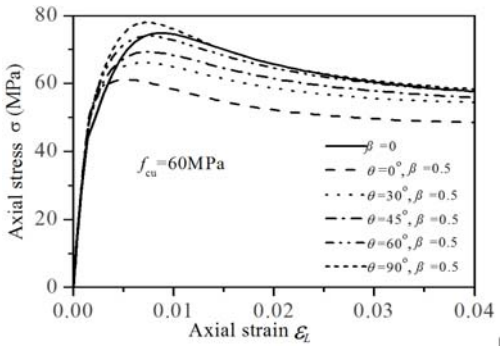


Fig. 19 Average axial stress-strain curve on the mid-section of the concrete with different notch orientation

notch width was 20 mm.

Fig. 18 shows the load-axial strain curves of specimens with different notch orientation. It is seen that the notch orientation had marginal influence on the stiffness of the inclined notched circular CFT stub columns but had significant influence on the ultimate bearing capacity. The bearing capacity of specimens with inclined notch and axial notch was similar when $\theta$ was small. With the increase of $\theta$, the bearing capacity of the specimens increased continuously. When $\theta$ reached 90°, in other words, the inclined notch became a circumferential notch, the bearing capacity of the specimen was the biggest and even slightly higher than that of the un-notched specimens. It indicates that the bearing capacity of specimens with axial notch is the lower limit while the bearing capacity of specimens with circumferential notch is the upper limit. And the bearing capacity of specimens with inclined notch is just in between of them.

Fig. 19 presents the average axial stress-strain curves at the mid-section of concrete of the specimens with different notch orientation. It can be observed that, with the increase of the angle $\theta$, the average axial stress at the mid-section of concrete was increased, which was at the minimum value when specimen had an axial notch and at the maximum value when specimen had a circumferential notch. And this maximum value was slightly higher than that of the un-notched specimen. It shows that the steel tube with axial notch had the least composite action on concrete while the steel tube with circumferential notch had the most composite action on concrete. Moreover, the composite action of steel tube with inclined notch was in between two of them and would be increased with the increase of notch orientation angle $\theta$.

Fig. 20 shows breakdown stress contours of specimens with different notch orientation. It is found that the specimens with axial notch experienced the largest buckling deformation of the steel tube where stress concentration was more pronounced. While the smallest buckling deformation of steel tube was noticed in the notched specimens with circumferential notch where the stress of steel tube was distributed evenly, and the stress of steel tube with inclined notch was in between them.

## 4. Theoretical method

In order to study the level of reduced bearing capacity of circular CFT stub columns with axial notch, the coefficient SI of bearing capacity was introduced, which is defined as the ratio of the bearing capacity $N_{uc}$ of the specimens with axial notch and the bearing capacity $N_u$ of the un-notched

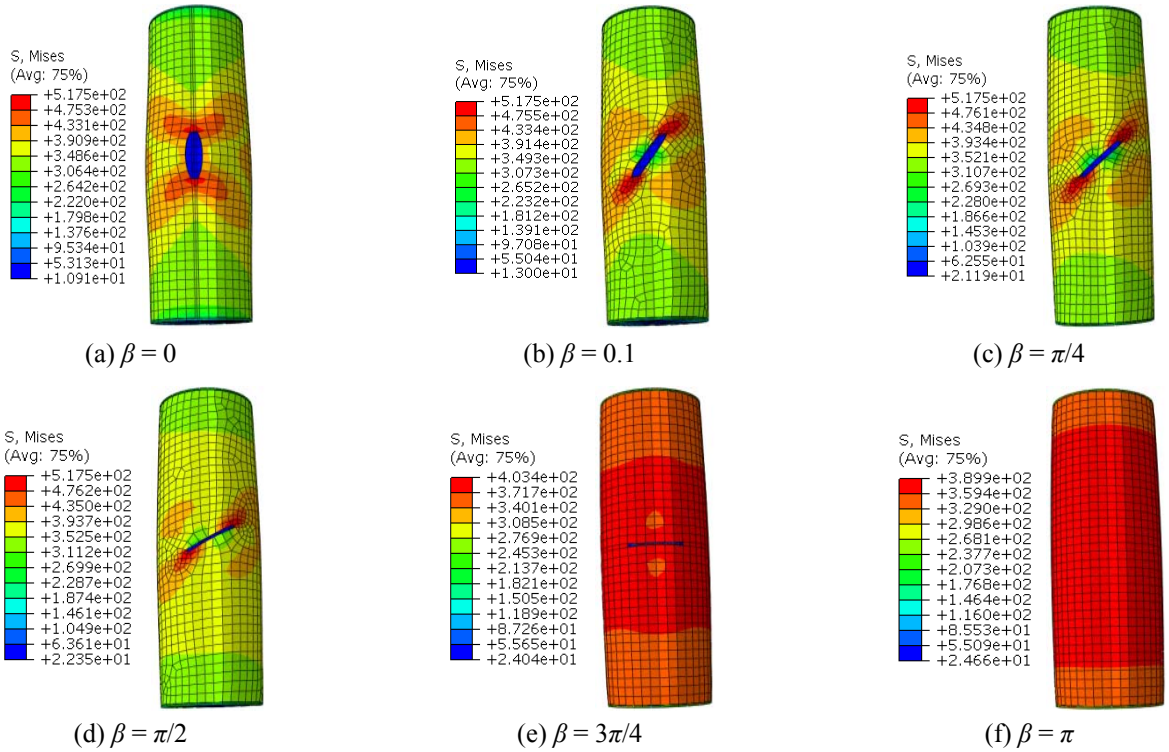


Fig. 15 Breakdown stress contours of specimens with different circumferential notch length

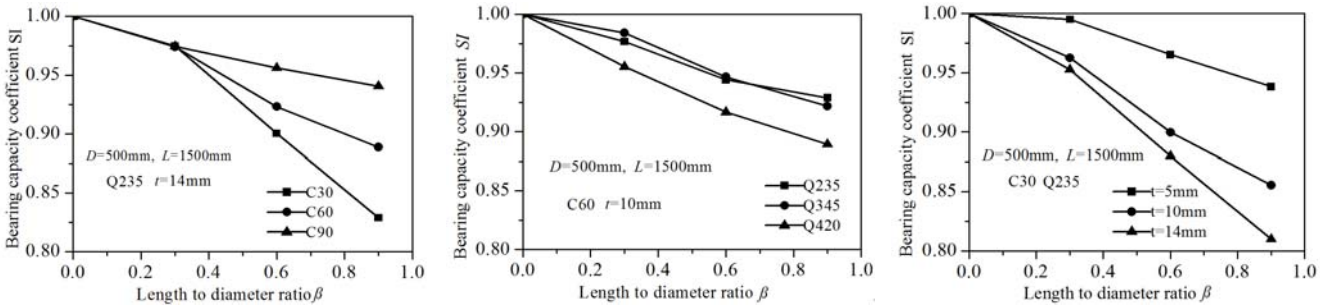


(a) Concrete strength (b) Steel strength (c) Steel ratio

Fig. 21 Effects of each parameter on *SI*

specimens with all other conditions

$$SI = \frac{N_{\text{uc}}}{N_{\text{u}}} \tag{3}$$

To investigate the effects of parameters, including aperture ratio, concrete strength, steel strength, and steel ratio on coefficient *SI* of circular CFT stub columns with axial notch under axial compression, parametric study was conducted, and the steel tube diameter *D* was selected to be 500 mm and the specimen length *L* was taken as 1500 mm. A total of 96 specimens were established for parametric analysis.

Fig. 21 shows effects of various parameters including concrete strength, notch length to diameter ratio ($\beta$), steel strength, and steel ratio on the coefficient *SI* of circular CFT stub columns with axial notch under axial compression. As can be seen from Fig. 21(a), the greater the $\beta$ is, the smaller the coefficient *SI* would be, and the greater the concrete strength is, the larger the bearing capacity influence coefficient *SI* would be. In Fig. 21(b), the coefficient *SI* is corresponding to Q235 and Q345 steel are similar but much larger than that corresponding to Q420. It indicates that the coefficient *SI* may decrease with the increase of steel strength above Q345. In addition, the larger the steel ratio is, the smaller the coefficient *SI* would be as shown in Fig. 21(c).

The following mathematical form for bearing capacity of the circular CFT stub columns under axial compression was proposed by Ding *et al*. (2011b)

$$N_u = f_c A_c (1 + 1.7\Phi) \tag{4}$$

where $\Phi$ is a confinement index, and equals to $A_s f_s/(A_c f_c)$. 1.7 is a confinement coefficient which embodies the composite action between the steel tube and the core concrete. For the steel tube with axial notch, the composite action on concrete is reduced and confinement coefficient decreases, therefore, the bearing capacity of circular CFT stub columns with axial notch is assumed as

$$N_u = f_c A_c (1 + k_1\Phi) \tag{5}$$

where $k_1$ is the confinement coefficient of circular CFT stub columns with axial notch. From the parametric analysis conducted above, it can be observed that the main parameter affecting $k_1$ is the notch length to diameter ratio $\beta$. And the relationship between confinement coefficient $k_1$ and aperture ratio $\beta$ of 96 specimens is shown in Fig. 22 and can be regressed as

$$k_1 = 1.7 - 0.5\beta \tag{6}$$

Substituting Eq. (6) into Eq. (5), the calculation formula of ultimate bearing capacity for circular CFT stub columns with axial notch can be obtained as

$$N_u = f_c A_c [1 + (1.7 - 0.5\beta)\Phi] \tag{7}$$

The comparison of FE results of $N_{u1}$ of 96 specimens versus $N_{u2}$ obtained by Eq. (7) is shown in Fig. 23, with the

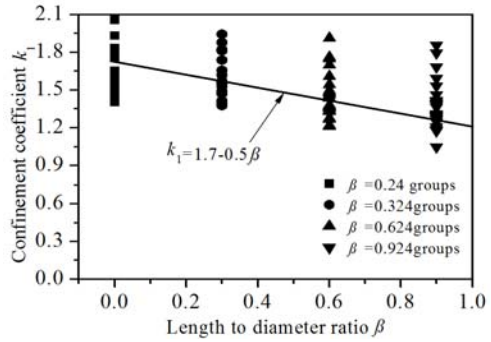


Fig. 22 Relationship between confinement factor and notch length-diameter ratio of axial notched specimens

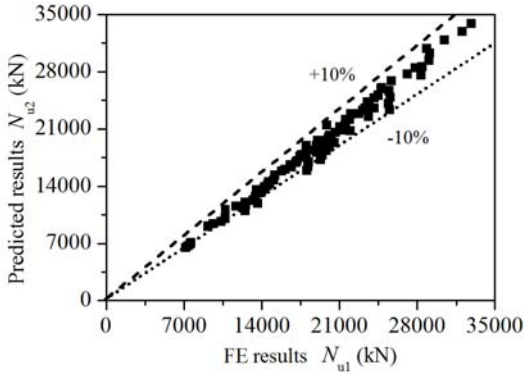


Fig. 23 Comparison of calculated result of $N_{u1}/N_{u2}$

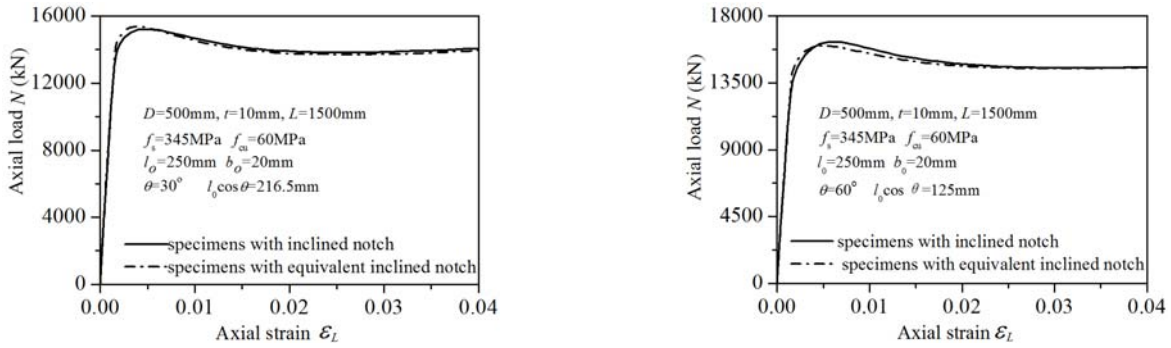


(a) $\theta = 30°$ (b) $\theta = 60°$

Fig. 24 Comparisons of load-strain response of inclined notched examples and equivalent axial notched specimens

average $N_{u1}/N_{u2}$ values being 1.036 and the dispersion coefficient being 0.042. As shown in Fig. 23, the FE results showed good agreement with the values obtained by Eq. (7), with the differences being controlled within 10%.

### 4.1 Effect of axial notch quantity and notch orientation

As found from Section 2.1, when $\beta$ was the same, the bearing capacity of steel tube in the mid-section with a single notch was the smallest among the specimens with different axial notch quantity and notch orientation. In order to consider the effects of axial notch quantity and notch orientation on the load bearing capacity, the most unfavorable situation could be adopted for the calculation. Namely, the bearing capacity of steel tube in the mid-section with a single axial notch could provide a conservative prediction on the load bearing capacity of the columns with different axial notch quantity and notch orientation. Therefore, the bearing capacity could be calculated by Eq. (7), where $\beta$ is the holistic notch length to diameter ratio of specimens, obtained by the superposition of each notch length to diameter ratio.

### 4.2 Effect of circumferential notch

From the analysis result in Fig. 11, slotting a circumferen-tial notch at the mid-section of steel tube reduces the axial stiffness and increases the ultimate bearing capacity of the specimens, bearing capacity of circular CFT stub columns under axial compression with circumferential notch could be approximately equivalent to the ultimate

Table 1 Specimen details, and comparison of load bearing capacity from different methods

| Specimens | Ref. | $\theta$ (°) | $D\times t$ (mm) | $L$ (mm) | $f_{cu}$ (MPa) | $f_s$ (Mpa) | $l_0\times b_o$ (mm) | $\beta$ | $N_{u0}$ (kN) | $N_{u1}$ (kN) | $N_{u2}$ (kN) | $N_{u0}/N_{u1}$ | $N_{u0}/N_{u2}$ |
|---|---|---|---|---|---|---|---|---|---|---|---|---|---|
| CN-2 | Chang (2013) | 0 | 111.64×1.90 | 400 | 56.7 | 261.3 | 48×6 | 0.43 | 702.5 | 679.5 | 660.2 | 1.034 | 1.064 |
| CN-3 | | 0 | 111.64×1.90 | | 56.7 | 261.3 | 36×6 | 0.32 | 654.1 | 689.2 | 669.4 | 0.949 | 0.977 |
| ND-4 | | 30 | 111.64×1.90 | | 56.7 | 261.3 | 36×6 | 0.32 | 647.8 | 653.1 | 673.1 | 0.992 | 0.962 |
| ND-5 | | 60 | 111.64×1.90 | | 56.7 | 261.3 | 32×6 | 0.29 | 649.5 | 635.8 | 684.7 | 1.022 | 0.949 |
| LN-7 | | 90 | 111.64×1.90 | | 56.7 | 261.3 | 13×6 | 0.12 | 672.2 | 702.4 | 697.0 | 0.957 | 0.964 |
| LN-8 | | 90 | 113.64×1.90 | | 56.7 | 259.6 | 15×6 | 0.13 | 994.6 | 967.4 | 912.5 | 1.028 | 1.090 |
| LN-9 | | 90 | 111.64×1.90 | | 56.7 | 261.3 | 26×6 | 0.23 | 659.8 | 668.4 | 697.0 | 0.987 | 0.947 |
| LN-10 | | 90 | 111.64×1.90 | | 56.7 | 259.6 | 21×6 | 0.19 | 937 | 974.5 | 836.6 | 0.962 | 1.120 |
| LN-11 | | 90 | 111.64×1.90 | | 47.8 | 261.3 | 33×6 | 0.30 | 622.9 | 645.4 | 623.6 | 0.965 | 0.999 |
| LN-12 | | 90 | 111.64×1.90 | | 47.8 | 261.3 | 42×6 | 0.38 | 579.2 | 592.1 | 623.6 | 0.978 | 0.929 |
| LN-13 | | 90 | 111.64×1.90 | | 56.7 | 261.3 | 44×6 | 0.39 | 634.9 | 678.9 | 697.0 | 0.935 | 0.911 |
| LN-14 | | 90 | 111.64×1.90 | | 56.7 | 261.3 | 84×6 | 0.75 | 579 | 569.4 | 562.1 | 1.017 | 1.030 |
| LN-15 | | 90 | 113.64×3.64 | | 56.7 | 261.3 | 84×6 | 0.74 | 898.6 | 924.3 | 953.7 | 0.972 | 0.942 |
| SZ5S4A2 | Yu (2007) | 0 | 219×4.74 | 650 | 50.5 | 350 | 20×10 | 0.09 | 3160 | 3342 | 3186.3 | 0.946 | 0.992 |
| SZ5S3A2 | | 0 | 219×4.73 | 650 | 42.6 | 350 | 20×10 | 0.09 | 3150 | 3329 | 2942.4 | 0.946 | 1.071 |
| SZ3S6A2 | | 0 | 165×2.76 | 510 | 50.5 | 350 | 20×10 | 0.12 | 2060 | 2198 | 1791.3 | 0.937 | 1.150 |
| SZ3S4A2 | | 0 | 165×2.74 | 510 | 57 | 350 | 20×10 | 0.12 | 1785 | 1895 | 1695.3 | 0.942 | 1.053 |
| Average values | | | | | | | | | | | | 0.975 | 1.009 |
| Dispersion coefficient | | | | | | | | | | | | 0.034 | 0.071 |

bearing capacity of un-notched circular CFT stub columns, which can be obtained in Eq. (4).

### 4.3 Effect of inclined notch

Bearing capacity of axial notched circular CFT stub columns was reduced the most compared with un-notched specimens and those with circumferential notches. The inclined notch could be considered as axial notch with an equivalent axial notch length at $l_0\cos\theta$. Fig. 24 shows load-axial strain curve of specimens with different notch orientation and with equivalent axial notches. As the figure shown, the stiffness, ultimate bearing capacity, residual bearing capacity, ductility and other mechanical properties of axial notched specimens were similar to that of the inclined notched specimens that have equivalent axial notch length. Therefore, practical calculation formula of the ultimate bearing capacity for circular CFT stub columns with inclined notch can be expressed as

$$N_u = f_c A_c[1+(1.7-0.5\beta\cos\theta)\Phi] \quad (8)$$

In summary, the practical calculation formula of bearing capacity for the circular CFT stub columns with axial notch, circumferential notch and inclined notch can be unified to an expression as Eq. (8).

Total 17 experimental results from Yu *et al*. (2007) and Chang *et al*. (2013b) on the notched circular CFT stub columns under axial compression were used here to verify the proposed formula and the comparison results are listed in Table 1. The comparison between the test results $N_{u0}$, FE modeling results $N_{u1}$ and $N_{u2}$ calculated by Eq. (8) shows that the average ratios of $N_{u0}/N_{u1}$ of all specimens is 0.975 with a dispersion coefficient of 0.034 and the average ratio of $N_{u0}/N_{u2}$ is 1.009 with a dispersion coefficient of 0.071. The comparison indicated that the presented values calculated by Eq. (8) are in good agreement with FE modeling results and the test results, with the values calculated by Eq. (8) being conservative and slightly smaller than the test results while FE modeling results being slightly higher than the test results. Such reasonable agreement between the theoretical prediction and the experimental results indicates the applicability of the proposed theoretical method in predicting the bearing capacity of circular CFT stub columns subjected to axial compression with various notches in steel tubes.

## 5. Conclusions

In order to consider the defect columns under aggressive environment, this paper investigates the composite action of circular CFT stub columns under compression with axial, circumferential and inclined notches incorporated in steel tubes, respectively. With the FE models validated by experimental results, parametric study was conducted to understand the effects of different parameters on the mechanical behavior of circular CFT stub columns and also the composite action between the steel tube and the core concrete. With the aid of FEA, a practical computation formula with consideration of the composite action to predict the ultimate bearing capacity of CFT stub columns with notch in steel tubes was proposed and also verified through test results. More specifically, the main conclusions from this study can be drawn as below.

- Satisfactory agreement between the FE results and experimental results confirmed that the numerical models accurately predict the mechanical behaviors of circular CFT stub columns with various types of notches including axial, circumferential and inclined notches. The mechanical behaviors include the bearing capacity and residual strength.
- Slotting axially at the mid-section of the steel tube reduced the composite action exerted by steel tube on concrete and slotting circumferentially at the mid-section of the steel tube enhanced the composite action exerted by steel tube on concrete. In addition, slotting inclined at the mid-section of the steel tube could be equivalent to an axial slot with different length to diameter ratio.
- Circular CFT stub column under axial compression with multiple axial notches could be equivalent to a circular CFT stub column under axial compression with a single axial notch with the notch length equal to the superposition of the notch lengths from all axial notches.
- Based on parametric study and regression analysis, the theoretical formula of ultimate bearing capacity with confinement coefficient of 1.7-0.5$\beta$cos$\theta$ to take into account the composite action for circular CFT stub columns under axial compression with notches in different orientations was proposed. The considered orientations of the notches include axial, circumferential, and inclined. Reasonable agreement between the theoretical prediction and the experimental results were achieved.

## Acknowledgments

This research work was financially supported by the National Natural Science Foundation of China, Grant No.51578548.

## References

Baltay, P. and Gjelsvik, A. (1990), "Coefficient of friction for steel on concrete at high normal stress", *J. Mater. Civil Eng.*, **2**(1), 46-49.

Bhandari, J., Khan, F. and Abbassi, R. (2015), "Modelling of pitting corrosion in marine and offshore steel structures – A technical review", *Loss Prev. Proc.*, **37**(9), 39-62.

Chang, X., Ru, Z. and Zhou, W. (2013a), "Study on concrete-filled stainless steel carbon steel tubular (CFSCT) stub columns under compression", *Thin-Wall. Struct.*, **63**(3), 125-133.

Chang, X., Fu, L., Zhao, H.B. and Zhang, Y.B. (2013b), "Behaviors of axially loaded circular concrete-filled steel tube (CFT) stub columns with notch in steel tubes", *Thin-Wall. Struct.*, **73**(4), 273-280.

Ding, F.X., Ying, X.Y. and Zhou, L.C. (2011a), "Unified calculation method and its application in determining the

uniaxial mechanical properties of concrete", *Front. Archit. Civil Eng. China*, **5**(3), 381-393.
Ding, F.X., Yu, Z.W. and Bai, Y. (2011b), "Elasto-plastic analysis of circular concrete-filled steel tube stub columns", *J. Struct. Eng.*, **67**(10), 1567-1577.
Ding, F.X., Lu, D.R. and Bai, Y. (2016a), "Comparative study of square stirrup-confined concrete-filled steel tubular stub columns under axial loading", *Thin-Wall. Struct.*, **98**(1), 443-453.
Ding, F.X., Li, Z., Cheng, S.S. and Yu, Z.W. (2016b), "Composite action of octagonal concrete-filled steel tubular stub columns under axial loading", *Thin-Wall. Struct.*, **107**(10), 453-461.
Ding, F.X., Tan, L., Liu, X.M. and Wang, L.P. (2017), "Behavior of circular thin-walled steel tube confined concrete stun columns", *Steel Compos. Struct., Int. J.*, **23**(2), 229-238. DOI: doi.org/10.12989/scs.2017.23.2.229
Han, L.H., Yao, G.H., Chen, Z.P. and Yu, Q. (2005), "Experimental behavior of steel tube confined concrete (STCC) columns", *Steel Compos. Struct., Int. J.*, **5**(6), 459-484.
Han, H., Cheng, J., Taheri, F. and Pegg, N. (2006), "Numerical and experimental investigations of the response of aluminum cylinders with a cutout subject to axial compression", *Thin-Wall. Struct.*, **44**, 254-270.
Hibbitt, Karlson & Sorensen Inc. (2003), ABAQUS/standard User's Manual; Version 6.4.1, Pawtucket, RI, USA.
Huang, Y.S., Long, Y.L. and Cai, J. (2008), "Ultimate strength of rectangular concrete-filled steel tubular (CFT) stub columns under axial compression", *Steel Compos. Struct., Int. J.*, **8**(2), 115-128.
Javidruzi, M., Vafai, A., Chen, J.F. and Chilton, J.C. (2004), "Vibration, buckling and dynamic stability of cracked cylindrical shells", *Thin-Wall. Struct.*, **42**, 79-99.
Johansson, M. and Gylltoft, K. (2002), "Mechanical behavior of circular steel-concrete composite Stub columns", *J. Struct. Eng.*, **128**(8), 1073-1081.
Jullien, J.F. and Limam, A. (1998), "Effects of openings of the buckling of cylindrical shells subjected to axial compression", *Thin-Wall. Struct.*, **31**(1-3), 187-202.
Lu, Z.H. and Zhao, Y.G. (2010), "Suggested empirical models for the axial capacity of circular CFT stub columns", *J. Constr. Steel Res.*, **66**(6), 850-862.
Melchers, R.E. (2006), "Recent progress in the modeling of corrosion of structural steel immersed in Seawaters", *Infrastruct. Syst.*, **12**(3), 154-162.
Ottosen, N.S. and Ristinmaa, M. (2005), "12-common plasticity models", *The Mechanics of Constitutive Modeling*, 279-319.
Park, J.W. and Choi, S.M. (2013), "Structural behavior of CFRP strengthened concrete-filled steel tubes columns under axial compression loads", *Steel Compos. Struct., Int. J.*, **14**(5), 453-472.
Sultana, S., Wang, Y. and Sobey, A.J. (2015), "Influence of corrosion on the ultimate compressive strength of steel plates and stiffened panels", *Thin-Wall. Struct.*, **96**(11), 95-104.
Wang, Q.T. and Chang, X. (2013), "Analysis of concrete-filled steel tubular columns with "T" shaped cross section (CFTTS)" *Steel Compos. Struct., Int. J.*, **15**(1), 41-55.
Xiamuxi, A. and Akira, H. (2011), "Compression test of RCFT columns with thin-walled steel tube and high strength concrete", *Steel Compos. Struct., Int. J.*, **11**(5), 391-402.
Yu, Z.W., Ding, F.X. and Cai, C.S. (2007), "Experimental behavior of circular concrete-filled steel tube stub columns", *J. Constr. Steel Res.*, **63**(2), 165-174.